were not angiogenic at 100 times this concentration.

These observations suggest that the degradation of hyaluronic acid in developing or remodeling tissues may not only remove the antiangiogenic activity of the native hyaluronate but also produce fragments that are angiogenic. The mode of action of the hyaluronate degradation products has yet to be determined. However, hyaluronic acid is known to bind to and modulate the interaction of fibronectin with collagen (*12*), aggregate proteoglycans (*13*), and self-associate to a considerable degree (*14*). Hyaluronate oligosaccharides (similar in size to the angiogenic fragments) inhibit many of these interactions (*11, 12, 14*). Recently several proteins were isolated from the extracellular matrix and found to be able to bind to hyaluronate; they appear to be involved in structuring the extracellular matrix. It is reasonable to assume that hyaluronate fragments would also interfere with their function. Thus the stimulation of angiogenesis may be due to a "loosening" or disorganizing effect on the extracellular matrix and a weakening of cell-cell and cell-matrix interactions.

Electron microscopy has shown significantly more small vessels in ischemic areas of infarcted myocardium from animals treated with high doses of hyaluronidase than in such tissue from untreated animals (*15*). Furthermore, hyaluronate has been implicated in the invasive growth of tumors, which have been shown to produce hyaluronidase (*16*). In several disease conditions (rheumatoid arthritis, osteoarthritis, and diabetic retinopathy), vascularization occurs close to a hyaluronate-rich fluid. In rheumatoid arthritis a decrease in the molecular weight of joint fluid hyaluronate may be due in part to the action of hyaluronidase or oxygen radicals (*17*).

Although numerous angiogenic factors have been detected (*18*), none has been adequately characterized. We have now identified a new angiogenic factor and determined its size distribution. The ubiquitous presence of hyaluronate in tissues suggests that the native and degraded forms are important in the control of normal and pathological neovascularization. An understanding of the mode of action of these angiogenic fragments may enable us to modulate the angiogenic process.

D. C. West
I. N. Hampson
F. Arnold
S. Kumar

Christie Hospital,
Manchester M2O 9BX, England

References and Notes

1. B. P. Toole, in *Cell Biology of the Extracellular Matrix*, E. D. Hay, Ed. (Plenum, New York, 1981), pp. 259–294; L. A. Culp, *Curr. Top. Membr. Transp.* **11**, 327 (1978).
2. H. Muir, *Biochem. Soc. Trans.* **11**, 613 (1984); E. Turley and D. Moore, *Biochem. Biophys. Res. Commun.* **121**, 808 (1984).
3. B. P. Toole, in *Neuronal Recognition*, S. H. Baronades, Ed. (Plenum, New York, 1976), pp. 275–329; E. Belsky and B. P. Toole, *Cell Differ.* **12**, 61 (1983).
4. R. N. Feinberg and D. C. Beebe, *Science* **220**, 1177 (1983).
5. E. A. Balazs and Z. Darzykiewicz, in *Biology of Fibroblast*, E. Kulonen and J. Pikkarainen, Eds. (Academic Press, New York, 1973), pp. 237–252; N. Rydell and E. A. Balazs, *Clin. Orthop.* **80**, 25 (1971).
6. S. Kumar *et al.*, *Lancet* **1984-II**, 364 (1984).
7. J. C. Houck and C. M. Chang, *Inflammation* **3**, 447 (1979).
8. T. Yamagata *et al.*, *J. Biol. Chem.* **243**, 1523 (1968).
9. I. N. Hampson and J. T. Gallagher, *Biochem. J.* **221**, 697 (1984).
10. J. T. Gallagher *et al.*, *ibid.* **215**, 107 (1983).
11. S. Eriksson *et al.*, *Exp. Cell. Res.* **144**, 223 (1983).
12. K. M. Yamada, in *Cell Biology of the Extracellular Matrix*, E. D. Hay, Ed. (Plenum, New York, 1981), pp. 9–114; H. Hormann and V. Jelinic, *Hoppe-Seyler's Z. Physiol. Chem.* **362**, 87 (1971).
13. V. C. Hascall and Heinegard, *J. Biol. Chem.* **249**, 4242 (1974).
14. E. R. Morris, D. A. Rees, E. J. Welsh, *J. Mol. Biol.* **138**, 383 (1980).
15. R. A. Kloner, M. C. Fishbain, D. Maclean, *Am. J. Cardiol.* **40**, 43 (1977).
16. B. P. Toole, B. Chitra, J. Gross, *Proc. Natl. Acad. Sci. U.S.A.* **76**, 6299 (1979).
17. J. C. Caygill, in *Carbohydrate Metabolism and Its Disorders*, F. Dickens, P. J. Randle, W. J. Whelan, Eds. (Academic Press, New York, 1968), vol. 1, pp. 223–263; E. R. Berman and M. Voaden, in *Biochemistry of the Eye*, C. N. Graymore, Ed. (Academic Press, New York, 1970), pp. 373–471; H. Furthmayr and R. Timpl, *Int. Rev. Connect. Tissue Res.* **7**, 61 (1976).
18. A Fenselau, Ed., *Oncology Overview* (National Cancer Institute, Bethesda, Md., 1983).
19. The technical help of J. Heslop and N. Evans is gratefully acknowledged. We also thank R. Stoddart and D. Harnden for their valuable advice and criticism. D.C.W. is supported by the Medical Research Council. S.K. is in receipt of grants from the Wellcome Foundation and British Heart Foundation.

13 September 1984; accepted 25 March 1985

Dragonfly Flight: Novel Uses of Unsteady Separated Flows

Abstract. *Studies of insect flight have revealed novel mechanisms of production of aerodynamic lift. In the present study, large lift forces were measured during flight episodes elicited from dragonflies tethered to a force balance. Simultaneously, stroboscopic photographs provided stop-action views of wing motion and the flow-field structure surrounding the insect. Wing kinematics were correlated with both instantaneous lift generation and vortex-dominated flow fields. The large lift forces appear to be produced by unsteady flow-wing interactions. This successful utilization of unsteady separated flows by insects may signal the existence of a whole new class of fluid dynamic uses that remain to be explored.*

Many insect species exhibit flight behaviors not readily explained by conventional steady-state aerodynamics (*1, 2*). Using high-speed photographic records of hovering chalcid wasps, Weis-Fogh (*2*) observed a wing upstroke completed by a dorsal clap and a downstroke initiated by a flinging apart of the wing leading edges. These so-called "clap" and "fling" movements were purported to induce both temporally and spatially dependent circulations about the wings that accounted for large unsteady lift forces. The estimated lift values were consistent with the observed hovering behavior. Analytic evaluations (*3*) corroborated the postulated underlying unsteady fluid mechanics. Using physical models to simulate the Weis-Fogh mechanism, Maxworthy (*4*) visualized these unsteady separated flows and suggested that they play a larger role in the production of lift than had been predicted. Theoretical (*5*) and experimental (*6*) analyses have further characterized the influences of unsteady separated flow on the Weis-Fogh mechanism of lift production. These studies indicated that novel unsteady fluid mechanisms can be used by certain insects. Moreover, these unsteady separated flow mechanisms, based on the same wing geometry and kinematics, appear to generate more lift than do steady-state mechanisms.

In this study we correlated dragonfly wing kinematics with lift history and the structure of the surrounding flow field. This insect exhibits a proficient flight capability with relatively simple, fixed-geometry wings. Its major flight modes include stationary hovering or slow hovering in any direction, high-speed upward and forward flight, and gliding flight. Earlier studies (*2, 7*) indicated that, for dragonfly hovering, calculations based on steady-state aerodynamic theory do not produce the lift values necessary to counterbalance the weight of the insect (*8*). In fact, the large geometric attack angles of the wings characteristic of dragonfly hovering may result in a total separation of the boundary layer that precludes the use of steady-state mechanics.

In evaluating the mechanisms of dragonfly flight, physical characteristics were measured, wing kinematics were documented photographically, lift production was correlated with wing motions, and flow was visualized to reveal

associated perturbations in the flow field. The results indicated that the dragonfly generates and controls unsteady separated airflows to produce lift. The manner in which the dragonfly does so, however, differs from that reported for the chalcid wasp.

Twenty-one dragonflies (*Libellula luctuosa*) netted in habitats near the University of Colorado, Boulder (~1600 m above sea level), were used for this study. Within 1 hour of capture, each dragonfly was temporarily immobilized with chloroform (or cooled to approximately 10°C) to simplify measuring and tethering. The average total area of the two wing pairs on each insect was 16 ± 1 cm^2 (mean ± standard deviation) and the average body mass was 340 ± 36 mg, so that the typical wing loading was 2.1 ± 0.2 N m^{-2}. The ratios of the square of the wingspan to the wing area (aspect ratios) were between 8 and 9 for the front wings and between 6 and 7 for the rear wings. Such aspect ratios are typical of enhanced lift-to-drag ratios (due to reduced wing-tip effects) used in gliding flight. Ratios of wing thickness to chord thickness ranged from 0.01 to approximately 0.05, indicating that the dragonfly wing can be approximated by a Blasius flat-plate model.

Dragonflies were tethered with cyanoacrylate adhesive at the ventral aspect of the synthorax to a one-dimensional force balance so that vertical lifting forces could be measured during flight episodes. Thirty minutes after tethering, insects were placed in a zero-flow environment, and flight episodes lasting 2 to 3 seconds were elicited two to three times per minute over a total test time of 10 to 15 minutes. Throughout tests there was no change in lift force or wing dynamics of the insects. The output of the force balance was continuously monitored by oscilloscope, and stroboscopic photographs were taken simultaneously with a 0.4-msec flash (2900 beam candle power seconds) positioned 28 cm above the insect. A light-sensitive diode was used to indicate the instantaneous lift force corresponding to the visualized wing configuration (Fig. 1).

Resulting views of wing motions were similar to those observed for tethered (*9*) and free hovering (*7, 10*) dragonflies. Correlated patterns of lift generation were repeated approximately every 36 msec, so that wing-stroke and peak lift-force frequencies averaged 28 Hz. The basic motion of the wing tips was down and forward during downstrokes and up and rearward during upstrokes (Fig. 2, A and B). Viewed from the side, the upper

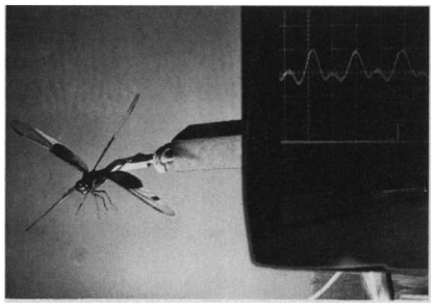

Fig. 1. A typical photograph used to correlate configurations of the dragonfly wings (left) with instantaneous lift generation (right). A spike in the lower oscilloscope trace generated by a light-sensitive diode marks the instantaneous force-balance output in the upper trace. Approximately three full cycles of the wings (hind pair marked in black near the tips) are represented by the three lifting cycles displayed on the upper oscilloscope trace. The horizontal oscilloscope sweep moves from right to left (total duration, 120 msec) in these mirror images.

half of the stroke plane of each wing pair was inclined 30° behind the vertical and the bottom half was 40° forward of the vertical. Geometric attack angles (acute angles measured from the stroke plane to the wing-surface plane) were estimated to be as large as 50° to 60° during downstrokes. During upstrokes wing attack angles decreased from the root to the wing tip because of spanwise twisting but still averaged a relatively large 20° to 30°. Rapid changes in attack angles were observed at the bottom of each downstroke, when the wing leading edges pitched up (supinated), and at the top of each upstroke, when the leading edges pitched down (pronated). The hind wings normally led the front pair through a stroke, with a phase-angle difference varying between 50° to 100° (Fig. 2, A and B). Average velocities of the wing-tips (~300 cm sec^{-1}) were larger during upstrokes (~350 cm sec^{-1}) than during downstrokes (~250 cm sec^{-1}). These values were obtained from stroboscopic visualizations that showed high reliability across tested specimens, with minor variances observed only in stroke rate and amplitude.

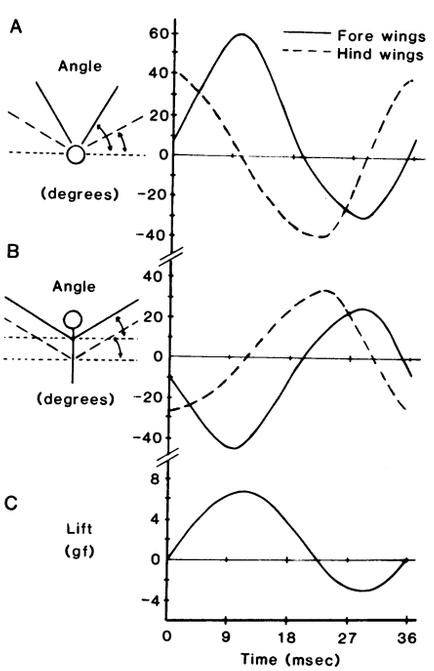

Fig. 2. A summary of an average dragonfly stroke cycle normalized to a 36-msec stroke period. Wing angles are summarized for observations from the front (A) and top (B) of the tethered dragonfly. Measurements of the corresponding lift (C) were estimated by subtracting the resonance values contributed by the mounting device (~55 Hz) from the total measurements of the force balance (1 gf = 9.81×10^{-3} N).

Force-balance measures revealed unsteady lift patterns, with smooth peaks of 5 to 7 gram-forces (gf) (4.9×10^{-2} to 6.9×10^{-2} N) during a typical test (Fig. 2C) (*11*). Thus, for an instant during each stroke cycle, a dragonfly weighing 0.34 gf produces lift forces 15 to 20 times its body weight. The average sustained lift was less than this but still amounted to more than twice body weight.

Correlations of lift history with wing kinematics (Fig. 2) showed that positive lift begins as the rear wings pronate and then accelerate into a downstroke. Lift increases steadily through the first half of the downstroke and reaches a maximum as the wings pass through the horizontal body plane. This lift maximum occurs 8 to 10 msec after a pronated rear wing slips past a supinated front wing. Lift drops toward zero during the second half of the rear-wing downstroke and becomes negative through the following upstroke. The first half of the front-wing downstroke coincides with a positive but decreasing lift, while the second half coincides with negative lift.

Flow visualization techniques were used to reveal the pattern of airflows interacting with the dragonfly during elicited flight episodes. A vaporized kerosene smoke was delivered (velocity, ~20 cm sec^{-1}) through Tygon tubing (1 cm in diameter) to a region directly in front of the insect. During flow visualization tests, limited to 5 minutes or less, behavior patterns did not differ from those observed in the absence of smoke. Flow visualizations, recorded photographically, revealed a prominent wake flow field behind the dragonfly. This wake described a symmetric wedge shape about the horizontal (apex angle

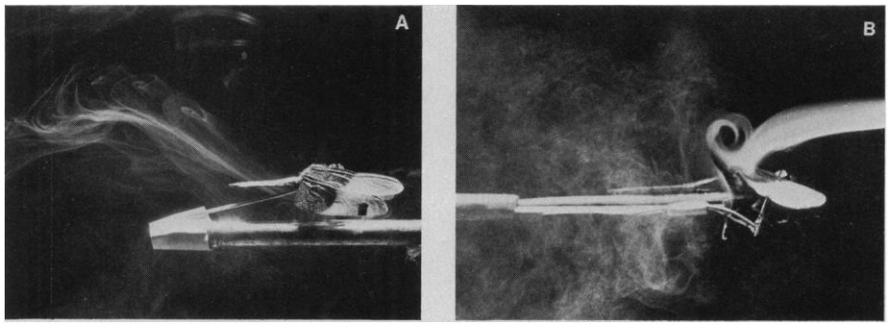

Fig. 3. (A) Stroboscopic photograph showing a typical wake flow field behind a tethered dragonfly. The insect is facing right with both wing pairs in the lower stroke plane. The mounting strut (thickness, ~12 percent wingspan) is positioned below and parallel to the dragonfly body to minimize interference with the induced flow field. Both a laminar vortex-dominated flow above the horizontal plane of the insect and a turbulent region below are apparent. The upper flow of this complex wake may arise from residual structures such as those in (B). (B) A multiple (four to five) exposure photograph of the phase-locked wing motion and associated flow field around the forewing (the other three wings have been surgically removed) of an automaton model (*13*) of the dragonfly (facing right). Wing motion is driven by electrical stimulation of flight-sensitive neuromuscular systems. When shed from the wing surface during a wing downstroke, vortex structures such as those shown gradually dissipate with convection away from the insect.

varying between 20° and 180°) which ranged from 5 to 15 cm in length. Although generally turbulent in appearance below the horizontal, above the horizontal the wake region often displayed a clearly defined character in which localized vortex stacking was evident (Fig. 3A). Previous model studies (*12*) suggest, and our follow-up studies (*13*) corroborate, that vortices and unsteady flow interactions are produced by dragonfly wing motions (Fig. 3B).

Nonsteady wing motions, such as rapid changes in wing attack angles and velocities, although necessary to support unsteady fluid mechanisms, are not sufficient to indicate a significant dependence on unsteady separated flows to generate lift. For example, during normal hovering as exhibited by many insects, the wings move in a horizontal figure-eight stroke plane at relatively small attack angles. For these insects, steady-state aerodynamic calculations yield lift values large enough to support the insect during hovering (*2*). However, in the dragonfly the stroke plane is nearly vertical, the wing pairs beat independently at large geometric attack angles, and the surrounding flow field is dominated by unsteady structures. Perhaps more important is that the tethered dragonfly produces a nonsteady lift history with large transient lift peaks 15 to 20 times its body weight. Even when time-averaged across a full stroke, our force balance data indicate that a tethered dragonfly generates a sustained lift two to three times its body weight, possibly indicating coefficients of wing lift, C_L, larger than the values of 2.3(2) and 6.1(7) predicted for sustained hovering. Such high C_L values are incompatible with steady-state aerodynamics at the associated Reynolds numbers of 1000 to 2000 (*8*). These data are suggestive of one or more unsteady fluid mechanisms that act in the production of lift for the dragonfly (*14*).

Unlike the chalcid wasp, dragonflies do not exhibit "clap" and "fling" wing movements. The front and rear wings are not latched together. Dragonflies operate their front and rear wing pairs independently, maintaining a specific phase relation between the wings. Visualization of the associated flow revealed an unsteady field different from that predicted and modeled for the "clap" and "fling" mechanism (*2, 4*) of the wasp.

The active changes in wing pitch (pronation and supination) initiating both downstrokes and upstrokes, respectively, have been suggested to play a role in unsteady lift generation for the dragonfly (*2, 7, 12*). The fluid dynamic mechanisms underlying such unsteady effects have not been described. Although the present force-balance recordings do not rule out such unsteady effects (*11*), the single large lift peaks that occur once in each stroke period suggest that lift generation is dominated by the integrated interactions between wings rather than by the unsteady effects elicited independently by each of four wings.

On the basis of the measurements of the forces generated during the wing-stroke motions of four wings, there may be a requirement for coordinated interactions between the front and rear wings, as has been speculated (*7*). The high positive lift that is generated immediately after a pronated rear wing slips downward past a supinated front wing (Fig. 2) may indicate that highly energetic vortex flows separate from the upward moving front wing and then interact with the rear wing to produce high lift. Although our data suggest a controlled movement of vortices between wing pairs, the details of these flows remain to be measured and correlated with lift production.

The tethered dragonfly may not be a precise model of the insect in free flight, but the similarities in wing movements are remarkable. That the tethered dragonfly generates high lift makes underlying fluid-wing mechanisms worthy of further investigation despite any departure from normal flight conditions. Also, such fluid mechanisms may exist initially near a dragonfly escaping freely from rest. Additional flow visualization studies together with a multidimensional force-balance analysis should help to clarify some of the finer details of these novel mechanisms of lift production (*13*).

It seems clear that the total flight behavior of most insects depends on both steady and unsteady fluid mechanisms. During any particular flight mode, one type of mechanism may predominate. The use of complex unsteady separated fluid mechanisms need not imply the existence of complicated wing geometry, motions, or control. The dragonfly generates large aerodynamic forces by means of rather simple wing structures and kinematics. Moreover, these wing kinematics and associated flow fields are different from those postulated by Weis-Fogh for the chalcid wasp. These observations suggest a number of different mechanisms for the generation and use of unsteady separated flows by insects. Whether such mechanisms might be useful on a larger scale at high Reynolds numbers remains to be seen (*15*).

CHRIS SOMPS
MARVIN LUTTGES
Department of Aerospace Engineering Sciences, University of Colorado, Boulder 80309

References and Notes

1. M. F. M. Osborne, *J. Exp. Biol.* **28**, 221 (1951).
2. T. Weis-Fogh, *ibid.* **59**, 169 (1973).
3. M. J. Lighthill, *J. Fluid Mech.* **60**, 1 (1973).
4. T. Maxworthy, *ibid.* **93**, 47 (1979).
5. R. H. Edwards and H. K. Cheng, *ibid.* **120**, 463 (1982).
6. G. R. Spedding and T. Maxworthy, *Bull. Am. Phys. Soc.* **28**, 1401 (1983).
7. R. A. Norberg, *Swimming and Flying in Nature* (Plenum, New York, 1975), vol. 2, pp. 763–781.
8. By steady-state definition, the lift coefficient, C_L, equals $L/\frac{1}{2}\rho V^2 S$ and the Reynolds number equals $\rho Vc/\mu$, where ρ and μ are the density and viscosity of the air, respectively, S is the wing surface area, and c is the average distance from the wing leading edge to the trailing edge. During hovering, each of the four wings of the dragonfly is assumed to develop an average lift force, L, equal to one-fourth the total insect weight. By assuming a simple harmonic wing motion and by making conservative estimates of the direction and magnitude of the velocities of

the induced flow, the average velocity, V, of the wing can be estimated. In the case of the dragonfly, even with conservative estimates of the stroke-plane angle and the portion of the stroke producing lift, C_L values calculated for the wing exceeded those measured from similarly shaped flat plates under steady-state conditions at equivalent Reynolds numbers.
9. L. E. Chadwick, *Bull. Brooklyn Entomol. Soc.* **35**, 109 (1940); J. W. S. Pringle, *Insect Flight* (Cambridge Univ. Press, Cambridge, 1957), p. 22.
10. M. W. Luttges, C. Somps, M. Kliss, M. Robinson, in *Proceedings of Workshop on Unsteady Separated Flow*, M. Francis and M. Luttges, Eds. (Colorado Associated University Press, Boulder, 1984), pp. 127–136.
11. Because of the mechanical low-pass filtering characteristics of the force balance used in these studies, lift variations with frequencies greater than 100 Hz were heavily damped. A newly designed three-dimensional force balance responsive to high frequencies indicates that high-frequency events may be superimposed on the dominant 25 to 30 Hz lift peaks reported here.
12. S. B. Savage, B. G. Newman, T.-M. Wong, *J. Exp. Biol.* **83**, 59 (1979).
13. Because of the relatively short duration of flight episodes (2 to 3 seconds) of varying wing-beat frequency (25 to 30 Hz), it is difficult to obtain detailed information about the local flow fields produced by self-initiated flight in the tethered dragonfly. To circumvent these problems, we presently use a modeling strategy in which electrical stimulation delivered to specific neuromuscular control centers of a tethered dragonfly produces stereotyped wing kinematics similar to those in self-initiated flight behavior. Visualization of the associated flow reveals an energetic, repeatable, unsteady vortex field interacting directly with the dragonfly wings.
14. On the basis of a typical wing-beat frequency of 28 Hz and a typical chord length of 1 cm, the nondimensional reduced frequency K ($\omega c/2V$, where ω is angular frequency) ranges from 0.3 to 3.0 for typical free-flight velocities of 3 to 0.3 m sec^{-1}, respectively.
15. W. J. McCroskey, *Annu. Rev. Fluid Mech.* **14**, 285 (1982); M. C. Robinson and M. W. Luttges, in *Proceedings of Workshop on Unsteady Separated Flow*, M. Francis and M. Luttges, Eds. (Colorado Associated University Press, Boulder, 1984), pp. 117–126; J. E. Lamar and J. F. Campbell, *Aerosp. Am.* **22**, 95 (1984).
16. We thank J. Button, W. Bank, and R. Meinzer for technical assistance. Supported in part by the U.S. Air Force Office of Scientific Research grant F4962083K0009.

26 June 1984; accepted 5 October 1984

Monitoring the Time Course of Cerebral Deoxyglucose Metabolism by ^{31}P Nuclear Magnetic Resonance Spectroscopy

Abstract. *The phosphorylation of 2-deoxyglucose by the mammalian brain is used as an index of the brain's energy metabolism. The results of phosphorus-31 nuclear magnetic resonance (^{31}P NMR) monitoring of conscious animals in vivo showed rapid phosphorylation of 2-deoxyglucose by brain tissue. The rate of phosphorylation as determined by ^{31}P NMR was consistent with results achieved by tracer methods using carbon-14–labeled 2-deoxyglucose. However, the disappearance of 2-deoxyglucose-6-phosphate was shown to be faster than that reported by tracer studies and occurred without alterations of intracellular pH and energy homeostasis. These results were confirmed by gas chromatography and mass spectroscopy. It is postulated that 2-deoxyglucose may be metabolized in several ways, including dephosphorylation by a hexose phosphatase.*

Brain neuronal activity requires large amounts of energy. Regions within the brain selectively increase or decrease energy utilization in a manner commensurate with behavioral changes, as is revealed by electroencephalography, evoked potentials, cerebral blood flow (*1*), and methods that employ metabolic substrates such as oxygen and glucose (*2*). The use of glucose analogs, including ^{14}C-labeled 2-deoxyglucose (2-dGlc) (*3*), has enhanced the applicability of techniques such as positron emission tomography and autoradiography. All the methods provide mutually confirming results. However, the basic assumptions of the analog methods have been challenged (*4*).

Phosphorus-31 nuclear magnetic resonance (^{31}P NMR) spectroscopy can monitor high-energy phosphorus metabolites—such as adenosine triphosphate (ATP), phosphocreatine (PCr), inorganic phosphate (P_i), and various phosphomonoesters (PME) including 2-deoxyglucose-6-phosphate (2-dGlc-6-P)—in living animals (*5*) (Fig. 1). The surface-coil radio frequency antenna, a small transmitter-receiver that can be placed over the intact skin of the anatomic region of interest, has allowed long-term, spatially localized observation of ongoing normal metabolic events (*6*). To study the accumulation of intracerebral 2-dGlc-6-P after a single intravenous injection of 2-dGlc in the conscious animal, we used surface-coil ^{31}P NMR to observe PME resonances before and after injection.

The subjects were 12 Sprague-Dawley rats (250 g in body weight), housed in group cages with free access to food, that had adapted to standing upright in an NMR probe while fully awake. For the experiments, the rats were deprived of food for 16 hours, after which their blood glucose content was measured. If the content for a particular rat was less than 100 mg/dl (5.6 m*M*), the animal was anesthetized with halothane and a catheter was inserted in the tail vein. After the rat awakened and could stand steadily on all four paws, pentobarbital (20 mg/kg) was delivered through the catheter, which was considered patent if the animal collapsed immediately. The rat was supported and restrained in an NMR probe. An oval, single-turn surface coil (~1.75 by 1 cm) was placed 1 mm above the cranium, and the rat was ascertained to be responsive by an active corneal reflex. The probe was inserted into an 8.5-T spectrometer (Bruker model WH 360) operating at a frequency of 145.8 MHz. Spectra for ^{31}P were collected in 5-minute blocks for 20 minutes before and 240 minutes after each rat received a bolus injection (0.25 cm^3; dose, 500 mg/kg) of either 2-dGlc (DG-NMR group, n = 4) or dextrose (DEX-NMR group, n = 4) in sterile water. A third group was not injected (NIC-NMR group, n = 4).

Statistical differences between relative concentrations of metabolite (as determined from peak heights) among groups over time were determined with an analysis of variance for repeated measures; the t-test was used to evaluate differences between two specific time blocks (*7*). In the DG-NMR group, the broad PME resonance rose after the injection, with maximum intensity at 40 minutes (Fig. 2A). A rapid decline then ensued, with the PME peak reaching half-maximum intensity 120 minutes af-

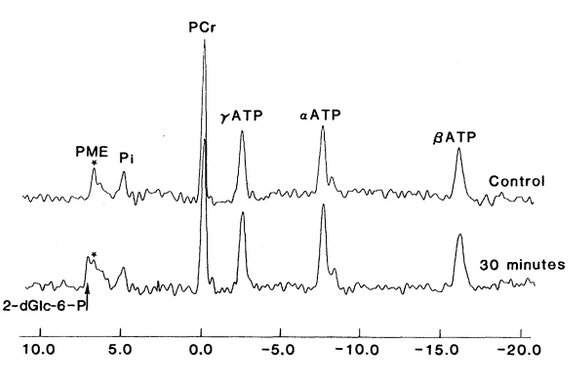

Fig. 1. Surface-coil ^{31}P NMR spectra from a rat treated with 2-dGlc. The normally intense baseline bone phosphate contribution was removed by convolution difference, and resolution-enhancement was carried out (*7*). In the control (upper) spectrum, resonances are identified as phosphomonoesters (PME, *), inorganic phosphate (P_i), phosphocreatine (PCr), and the γ-, α-, and β-phosphates of adenosine triphosphate (γATP, αATP, and βATP). In the lower spectrum [30 minutes after a bolus injection of 2-dGlc (500 mg/kg)], a new peak (↑) appeared at 7.11 parts per million, which is the chemical shift of 2-dGlc-6-P (*12*). Acquisition parameters: pulse width, 40 μsec at 100 W; spectral width, 10 KHz; 1024 data points; pulse repetition rate, 1 sec^{-1}; accumulation time, 10 minutes.